Life Prediction Under Biaxial Loading Based On The Growth Behaviour Of Short Cracks

by J. Prochotta and P. Neumann

Max-Planck-Institut für Eisenforschung GmbH, D-4000 Düsseldorf

Abstract

Biaxial fatigue tests were performed with thick walled tubular specimens made out of a ferritic structural steel and an austenitic stainless steel. Cyclic hardening/softening, crack initiation, crack growth, and cycles to failure were measured. The cyclic stress strain behaviour was found to be close to the Masing behaviour. Thus the ΔJ and the related damage parameter, Z_D, were used to describe the growth of intermediate cracks and the resulting cycles to failure. It was found that by using these parameters the data obtained in tension, torsion and biaxial tests can be described by one universal law.

1 Introduction

Life prediction for cyclic loading conditions has been very successful in laboratory tests using uniaxially loaded laboratory specimens. But the ultimate goal of fatigue research will always be the life prediction for real parts. They are, however, typically loaded under multi-axial conditions, especially at notches and other highly loaded areas. One simple possibility to transfer the results obtained in uni-axial loading to multi-axial loading is to replace the tensile components of stress and strain by the equivalent stresses and strains according to von Mises. Following Manson/Coffin the plastic equivalent strain would then be the essential parameter determining the cycles to failure, N_f. However, with such a simple approach many experimental findings cannot be described. Therefore, other parameters have been

proposed to improve the situation. Brown and Miller [1] proposed a generalized theory based on the maximum shear strain and on the tensile strain normal to the plane of maximum shear. A modification of this approach was proposed by Lohr and Ellison [2] by claiming that the strain which is normal to the specimen surface is of special importance. Kandil et al. [3] and Socie et al. [4] refined this approach in order to improve the description of mean stress effects.

A criterion which relys on the applied stresses was developed by Krempl [5]. Garrud [6] and Ellyin [7] proposed an energy criterium to determine the life under biaxial loading. The latter approach is closely related to the use of the cyclic J-integral, ΔJ, introduced by Dowling and Begley [8,9]. Wüthrich [10] proved that the ΔJ is indeed a path independent integral around the crack tip if the material shows Masing behaviour. Heitmann [11] used the ΔJ to derive a damage parameter suitable for life prediction for random uni-axial loading. The latter treatment seemed so promising that it will be tried in this paper to extend the ΔJ approach to proportional biaxial loading.

2 Experimental procedure

The experiments were done with an austenitic stainless steel, German grade X6CrNi1811 and with a ferritic construction steel, German grade StE 70. The chemical composition is given in **table 1**. Tubular specimens with an OD of 18 mm, a wall thickness of 4 mm, and a gauge length of 36 mm were used. Due to this large wall thickness elliptical surface cracks with a constant aspect ratio of 0.9 could be obtained up to a depth of 1 mm. The specimen geometry, which agrees with ASTM standards, is shown in **figure 1**. The specimens from the austenitic stainless steel were annealed in vaccum $p < 10^{-4}$ mbar and furnace cooled. The annealing parameters and the resulting grain sizes are shown in **table 2**. Twin boundaries were ignored for the determination of the grain size. The grain size of the ferritic steel was 13 μm, that of the austenite 50 to 450 μm, depending on the heat treatment.

Table 1: Chemical composition of the steels used (weigth-%)

	C	Cr	Ni	Si	Mn	P	S	Mo	Zr
X6 CrNi 18 11	0.05	17.5	10.6	0.45	1.6	0.02	0.002	0.02	—
StE-70	0.19	0.82	—	0.45	0.99	—	—	0.28	0.09

The surface finish of the specimens was a mechanical polish with 1 μm diamond paste. Additionally, the austenitic steel was electro-polished thereafter.

Since crack initiation can be observed only at the outer surface of the tubular specimen, crack initiation at the inner surface was avoided by reducing the surface roughness and introducing compressive stresses by honing. The tests were performed in a servo-hydraulic closed-loop tension-torsion system for a maximum load of 400 kN and a maximum moment of 4 kNm. The axial and torsional strains were measured with the help of strain gauges which were attached to the inner surface of the tubular specimens.

The control of the system and the recording of the data was performed by a PDP 11/73 computer from Digital Equipment. Stresses and strains were recorded with a resolution of 12 bit. The experiments were carried out with an instantaneous strain or stress control (reaction time 5 ms). Superimposed was an amplitude control with a reaction time of a few cycle times. In this way stress, total strain or plastic strain amplitude could be controlled independently for tension and torsion. Furthermore, the compliances for tension and torsion could be determined with an accuracy of 14 bit by compensating for the elastic slope of the hysteresis.

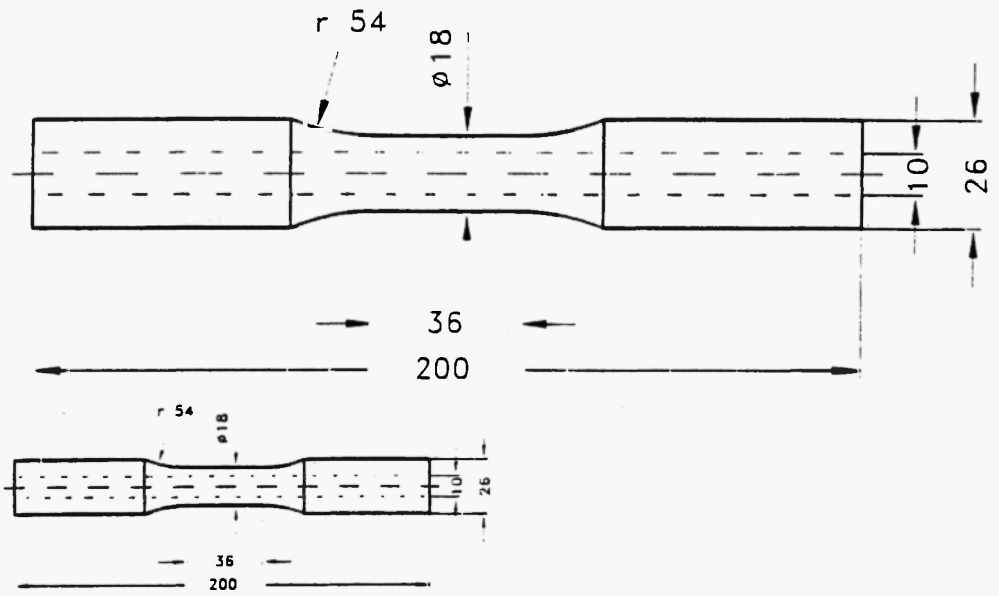

Figure 1: Specimen geometry.

A special problem is the undesired coupling of tension and torsion signals in stress as well as in strain. Since the coupling was almost linear and constant in the used ranges for the given load cell and a given specimen with its strain gauges, it could be compensated by a simple analog circuit, which introduced an appropriate small adjustable tension signal into the torsion signal and vice versa. If the actual forces become larger than 85 kN, a quadratic coupling term becomes noticeable but could still be neglected. Similarly, a quadratic coupling term became noticeable with the ferritic steel at small plastic strain amplitudes ($\Delta\epsilon_p < 10^{-4}$). It was also negligible for strain resolutions down to $3 \cdot 10^{-6}$.

Crack growth was measured in experiments with constant plastic strain amplitude and constant mean stress. For the determination of cyclic stress strain curves, incremental-step tests were performed during proportional biaxial tension-torsion loading. The number of steps varied between 40 and 80. Their height was not constant but was increased by a constant factor. In this way also in experiments with a large maximum amplitude sufficientely small plastic strains could be reached with the number of steps given above and in a figure with log scales the distances between the measured points are constant.

A few tension tests were carried out with solid cylindrical specimens for comparison with the tubular specimens, and no significant differences were found. In all biaxial tests the proportional loading was done with a constant plastic strain biaxiality. All tests were perfomed with a sinusoidal loading. The frequency was always chosen in such a way to avoid excessive heating of the specimen. In this way the frequency used ranged from 2 Hz down to 0.3 Hz. However, in tests with a large torsional amplitude, e.g. γ_t = 0.01, the frequency had to be reduced down to 0.01 Hz.

The crack growth was measured by taking replicas in regular intervals, typically 5% of the expected life time (de Lange [12] and Heroux [13]). With carbon shadowed

Table 2: Heat treatment and resulting grain size of the steel X6 CrNi 18 11

Temperature	Hold Time	Grain Size
1050 °C	60 min	50 μm
1100 °C	120 min	215 μm
1150 °C	180 min	450 μm

acetate replica cracks longer than 10μm could be detected in the optical microscope. From the surface length of the cracks the crack depth could be determined by measuring their aspect ratio on the fracture surface using fracture markings. By tracing back large cracks on the preceding replicas it was possible to determine the crack growth history back to the crack initiation.

The end of the life was determined by the appearance of cracks which are longer than 1 mm. In tension such cracks do significantly change the compliance which may be used to stop the test automatically. In torsion, however, surface crack lengths of more than 6 mm sometimes could not be detected by a change in the compliance.

3 Results

Since the strains were measured by strain gauges glued onto the specimen, the elastic moduli could be determined from the slope of the elastic range. **Table 3** gives the results.

In tension-torsion tests the stresses are not constant over the cross section of the specimen. Below yielding the torsional components are proportional to the radius. When plasticity commences at the outer surface, the radial distribution of torsional stresses becomes non-linear. Nadai has given a quantitative treatment of this problem for solid cylindrical specimens [14]. A solution for thick-walled cylindrical tubes was deduced by extending Nadai's solution by Neumann and Prochotta [15]. Let $T(\gamma_0)$ be the torque measured at the specimen as a function of the shear strain at the outer surface, γ_0. γ_0 is connected to the twist angle, θ, the radius r, and the length of the gauge section, l, by

$$\gamma = \frac{\theta r}{l}. \qquad (1)$$

Table 3: Elastic moduli of the steels used

	StE 70	X6 CrNi 18 11
E-Modul / *GPa*	215	204
G-Modul / *GPa*	84	80
Poisson's ratio	0.28	0.27

Nadai's solution for the full cylinder is given by

$$N(\gamma) = \frac{3T(\gamma) + \gamma \frac{dT(\gamma)}{d\gamma}}{2\pi r^3} \tag{2}$$

For tubular specimens with a ratio, c, between inner, r_i, and outer, r_0, radius

$$c = \frac{r_1}{r_0} \tag{3}$$

a solution according to [15] is given by

$$\tau(\gamma_0) = \sum_{\nu=0}^{n} c^{3\nu} N(c^\nu \gamma_0) + \frac{2G\gamma_0}{\pi r_0^3} \frac{c^{4(n+1)}}{1-c^4} \tag{4}$$

(4) is exact if n is taken large enough so that $c^n\gamma$ is in the elastic part of the torque-twist curve. For the specimens used here with c = 5/9, n = 2 is sufficient for all cases. (4) was used to calculate shear stresses from the torque-twist curve.

3.1 Cyclic Hardening

Figures 2 and 3 show the cyclic softening, i.e. a decrease of the torque amplitude, in ferritic steel experiments with constant plastic shear amplitude and zero mean

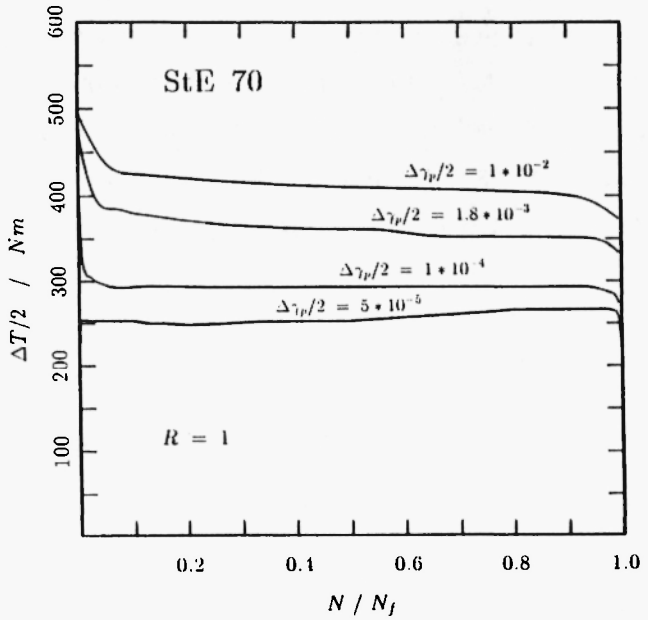

Figure 2: Amplitude of the torque as a function of the cycles during a torsion experiment with controlled plastic shear strain amplitude for the steel StE-70.

torque. After less than 10% of N_f the cyclic softening is complete and the torque amplitude saturates.

The austenic stainless steel shows cyclic softening/hardening at low/high shear strain amplitudes. At shear stress amplitudes beyond 0.7% no saturation is reached anymore. These small cyclic hardening/softening effects will always be neglected in the following by using stabilized hysteresis loops only.

Cyclic stress strain curves, CSSC, are difficult to determine in thick-walled tubular specimens because of the radial dependence of stresses and strains. In order to avoid these difficulties some specimens were produced with an inner diameter of 16.5 mm resulting in a wall thickness of 0.75 mm. Such specimens are thin-walled tubular specimens according to the ASTM standards. The differences between elastic and fully plastic calculations are less than 2% of the radial stress distributions. CSSCs were determined for both steels in multi-level tests with increasing amplitude under pure tension, pure torsion, and proportional tension-torsion load-

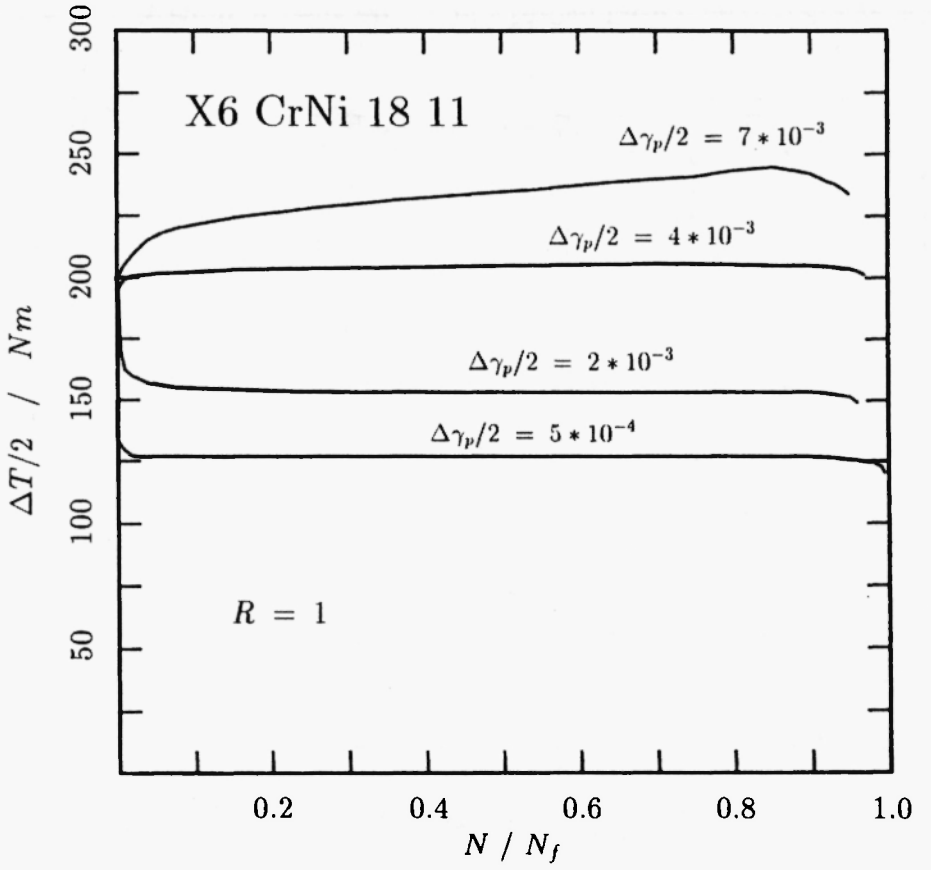

Figure 3: Amplitude of the torque as a function of the cycles during a torsion experiment with controlled plastic shear strain amplitude for the steel X6 CrNi 18 11.

ing with a constant plastic strain biaxiality $\lambda_{\epsilon_p} = \sqrt{3}$. Only stabilized hysteresis loops were evaluated. The results obtained from multi-level tests agreed well with the results of constant amplitude tests using different specimens. The scatter in the multi-level tests was, however, much smaller (**figures 4 and 5**).

The data for the austenite show no dependence on the biaxiality if the equivalent stresses are plotted vs. plastic equivalent strains. In the case of the ferritic steels deviations of this type occur only at plastic strains below 0.03%. Therefore a unified description of the biaxial CSSC in terms of the equivalent stresses and strains seems to be justified. The shape of the CSSC shows two regimes with different hardening exponents. Therefore, they may be described by a combination of two power laws according to

$$\frac{\Delta\bar{\epsilon}_v}{2} = \left(\left(\frac{K_S}{\Delta\bar{\sigma}/2} \right)^{1/n_S} + \left(\frac{K_L}{\Delta\bar{\sigma}/2} \right)^{1/n_L} \right)^{-1} \qquad (5).$$

The constants which are obtained from figures 4 and 5 are given in **table 4**.

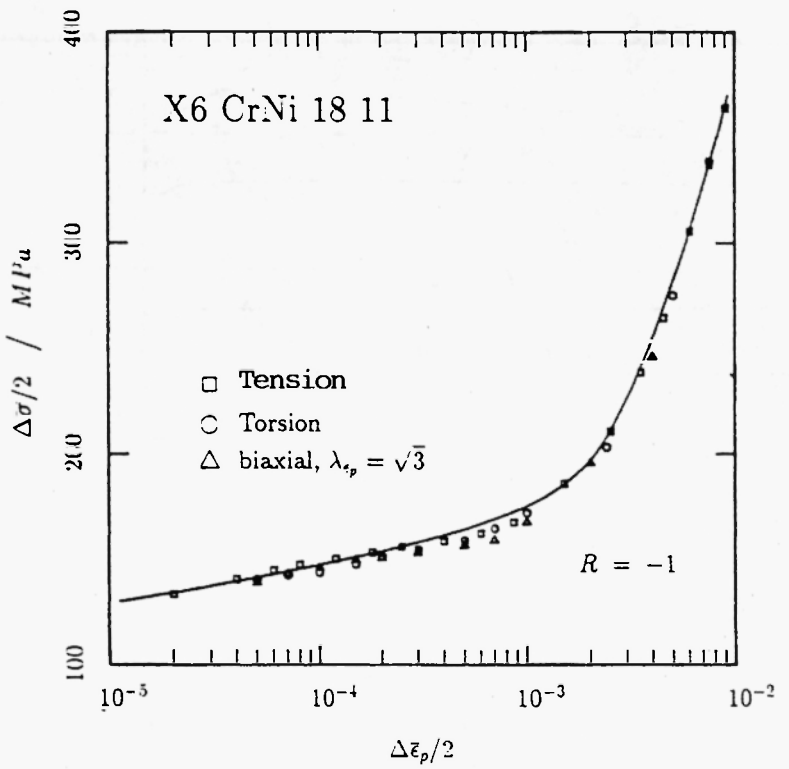

Figure 4: Cyclic stress strain curves according to multi level tests of the steel X6 CrNi 18 11.

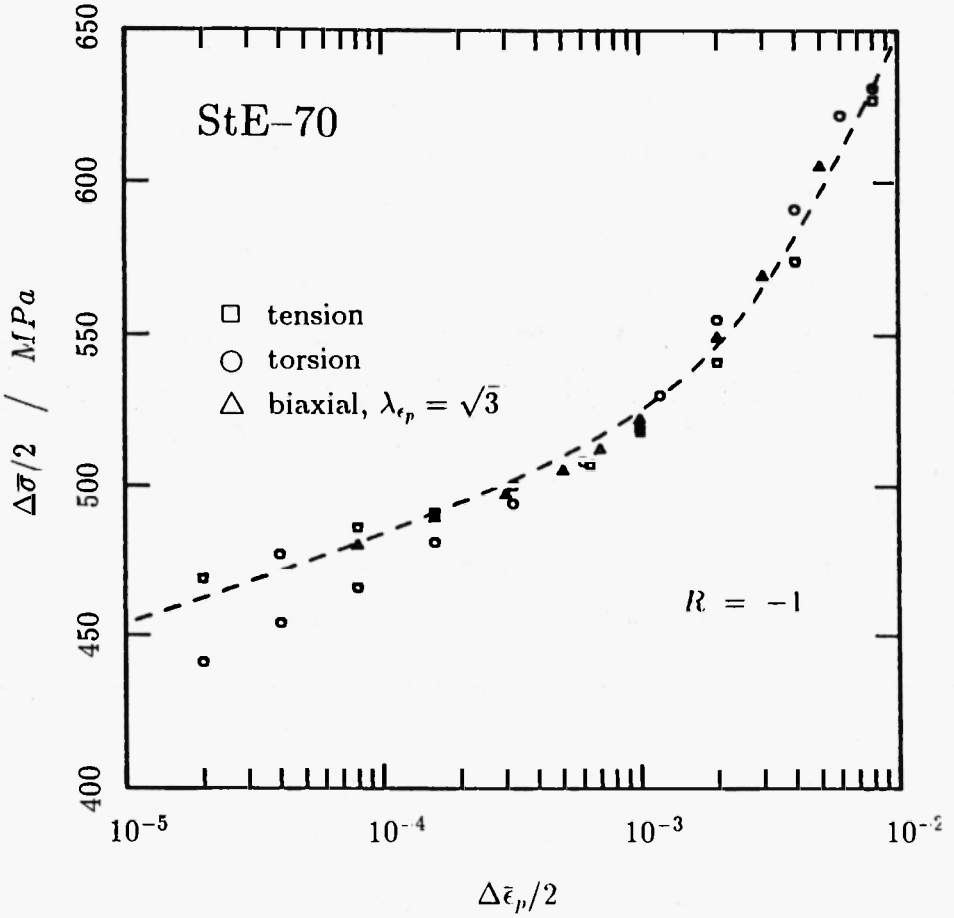

Figure 5: Cyclic stress strain curves according to multi level tests of the steel StE-70.

	StE 70	X6 CrNi 13 11
K_S / MPa	619	246
K_L / MPa	1148	2940
n_S	0.027	0.056
n_L	0.124	0.443

Table 4: Parameters of the cyclic plastic deformation behaviour according to equation (5)

3.1.1 Incremental Step Tests

With the ferritic steel incremental step tests with different maximum amplitudes were carried out. The increments in the equivalent plastic strain range were not constant but referred to a constant relative increase. In this way a large range of strains could be covered with good accuracy and a total number of 40 - 80 increments. It is obvious from the data in **figure 6** that they are independent of the biaxiality. The effect of the maximum amplitude can be cast in a single parameter K, the values of which are given in figure 6. With these values of K all incremental-step test data can described by

$$\Delta\epsilon_p/2 = \left(\frac{\Delta\bar{\sigma}/2}{K}\right)^{\left(\frac{1}{c_1 - c_2/K}\right)} \qquad (6)$$

with $c_1 = 0.25$ and $c_2 = 160$ MPa.

The dashed line in figure 6 shows the data obtained in multi-level tests with increasing amplitude (figure 5). There is good agreement at large amplitudes only.

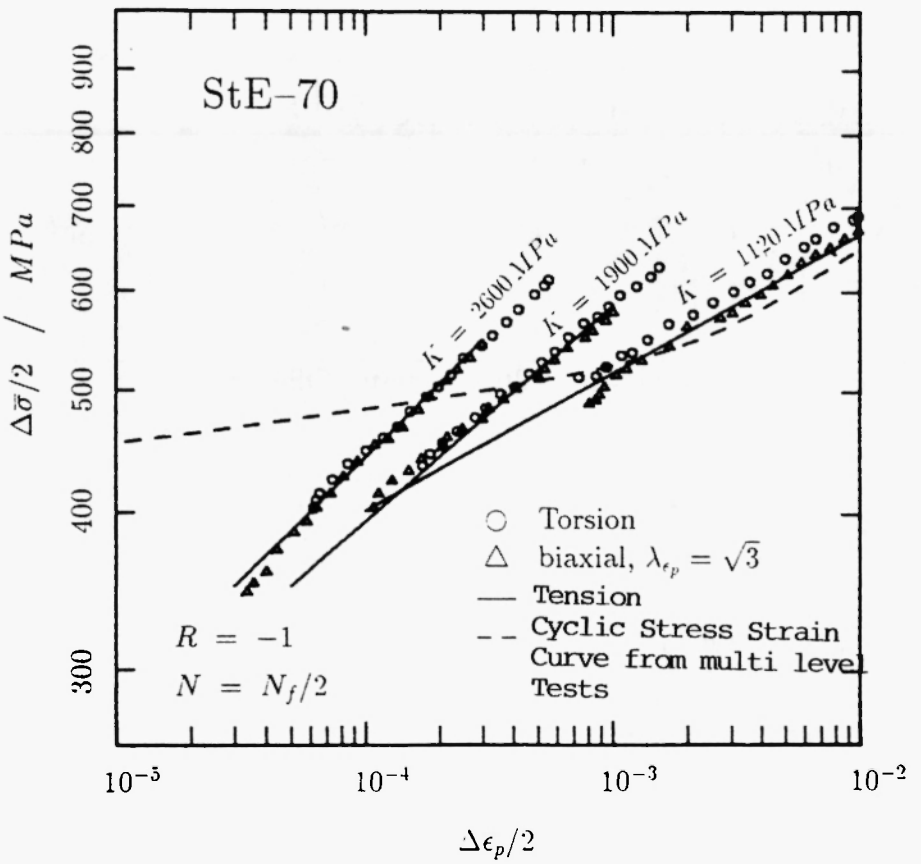

Figure 6: Cyclic stress strain curves from an incremental step tests with different maximum amplitudes and different biaxialities.

Since the incremental step test data depend on the maximum amplitude, there is no unique relation between stress and strain. If, however, the shape of individual stabilized hysteresis loops are compared with the CSSC curves from the incremental step tests, there is a good agreement as required by the Masing behaviour. Because of this the stress-strain relations obtained from incremental step tests were used for life-time predictions only.

3.2 Crack Initiation

Many studies have shown that crack initiation occurs at special sites: inclusions, grain boundaries, surface imperfections or slip bands with intrusions and extrusions. In the ferritic steel crack initiation at inclusions is dominant in biaxial tests. Heitmann [11] reach the same conclusion for uni-axial loading of the same material. For the stainless steel Ebi [16] and Tönnesen [17] have shown that at medium amplitudes slip band crack initiation is dominant. Near the fatigue limit slip bands are observed only in the intimate neigbourhood of twin boundaries. This result was explained by elastic imcompatibility stresses which occur at grain boundaries and also at twin boundaries due to elastic anisotropy (Neumann [18]). This model explains also the striking feature that in a stack of twin lamella only every other twin boundary is prone to cracking. These effects were also observed under biaxial loading. **Figure 7** gives an example.

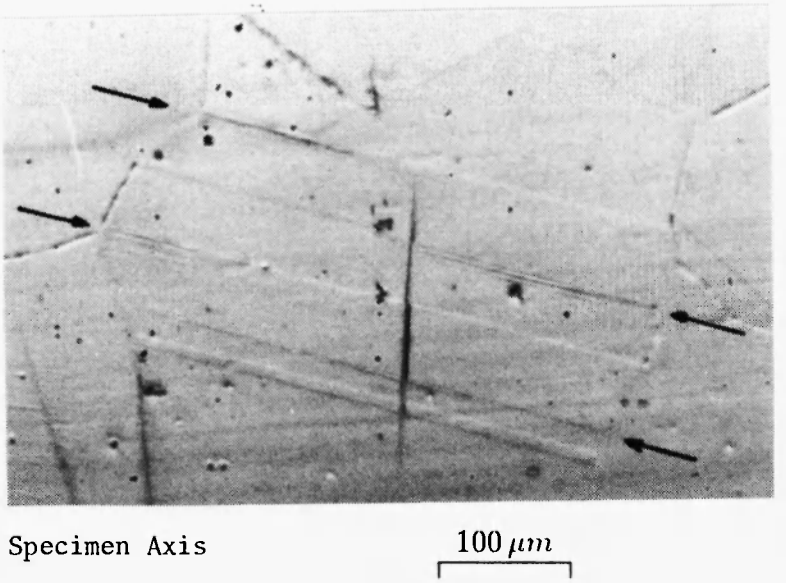

Figure 7: Initiation of cracks in X6 CrNi 18 11 at every other twin boundary.

3.3 Crack Growth

It is well known that after a certain distance of crack propagation along the slip plane (stage I of crack growth) the crack plane switches to the plane of maximum tensile stress (stage II of crack growth). In push-pull experiments all planes which form an angle of 45° against the tensile direction (**figure 8**) are maximum shear planes. Therefore, the change from stage I to stage II will, most likely, be detected only by inspection of the fracture surface in the interior of the specimen. In torsion experiments, however, there are only two sets of maximum shear planes and maximum tensile stress planes with different traces on the specimen surface such that the transition from stage I to stage II is readily observed on the surface. **Figure 9** shows a typical example in a torsion experiment in the low amplitude regime: When the crack, which starts on the horizontal maximum shear stress plane, reaches a certain length, the growth mode switches to stage II. At the point of transition almost all cracks do branch onto the two possible planes of maximum tensile stress. This behaviour can be explained as follows: At the critical length of the stage I crack a transition to both possible maximum tensile stress planes is equally likely. Under usual conditions branching would be suppressed because of the following: If the crack on one plane is, by chance, a little longer than the other, it will

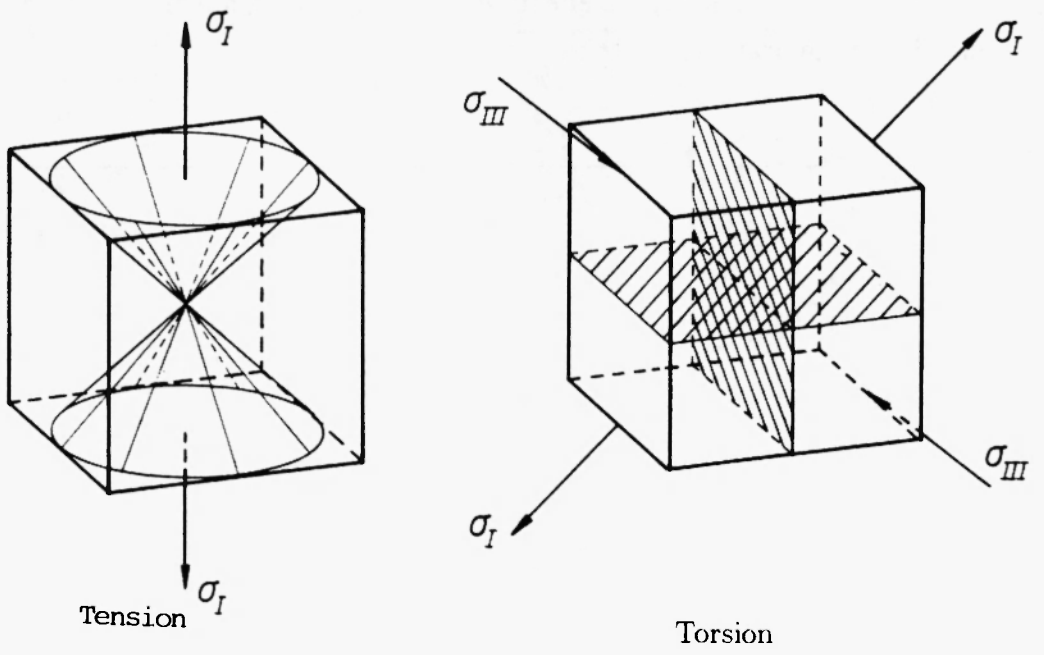

Figure 8: Planes of maximum shear stress in tension and torsion.

automatically reduce the stress concentration at the shorter crack, thus it will grow faster than the shorter crack, and will in this instable way soon outrun the shorter crack. This mechanism does not work in the torsion case. Both cracks will always grow when the tensile stress is maximum across their crack plane. This occurs, however, in the two different half cycles of the loading cycle. When one crack is opened in tension, the other will be closed by the compressive normal stress on its crack plane. In this sense both crack branches can grow independently in the two different parts of the loading cycles.

The appearance of this kind of branching pattern critically depends on the number of crack nuclei formed. In high amplitude loading (range I in figure 10) a large number of crack nuclei is formed at the surface. Before the critical crack length for stage II crack growth is reached, neighbouring cracks start to interact and therefore long cracks are formed by linkage of many small stage I cracks. In an intermediate range II patterns resembling the typical crack branching configurations occur (**figure 10**). However, these do not form by stage II crack growth but by linkage of stage I cracks in an average direction of stage II cracks which gives the cracks a stair-like course.

More or less the same behaviour was observed in the austenite. However, the ranges I and II of figure 10 are shifted to larger strains. Below 0.5% range III-beha-

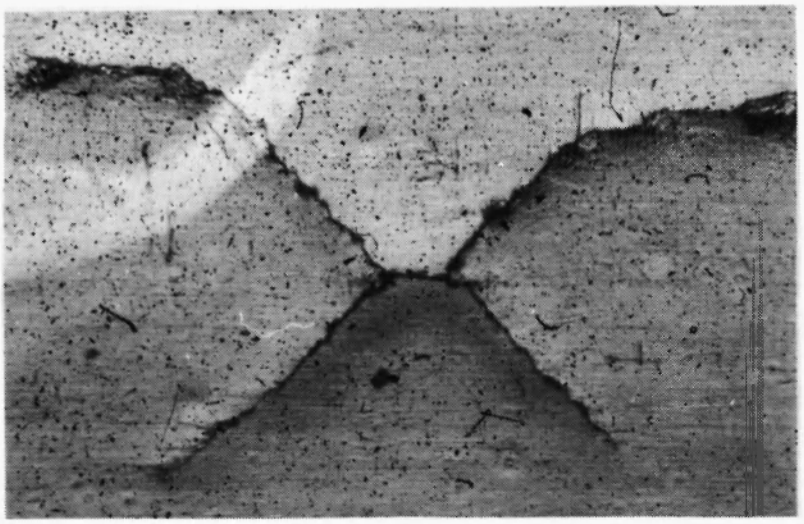

Figure 9: Crack growth in StE-70 during torsion, range III (fig. 10).
$\Delta\gamma_p/2 = 7.5 * 10^{-5}$, $N_{1\ mm} = 149000$.

viour is found. Because of the larger grain size and the well defined slip planes in the austenite, a pure stage II crack growth is disturbed considerably by the interaction with slip bands and grain boundaries. **Figures 11 and 12** give examples of cracks in the austenite. A similar behaviour was described by Bannantine and Socie [19] in the stainless steel AISI 316.

The growth of individual cracks can be obtained only in the high-cycle fatigue regime because then the crack nuclei are far enough apart. Short cracks which grow in stage I show a crack growth rate which is independent of the crack length. When the transition to stage II occurs there is a drop in the crack growth rate followed by a strong increase in growth rate which is slowed down when the crack depth becomes comparable with the wall thickness. **Figure 13** shows a typical behaviour.

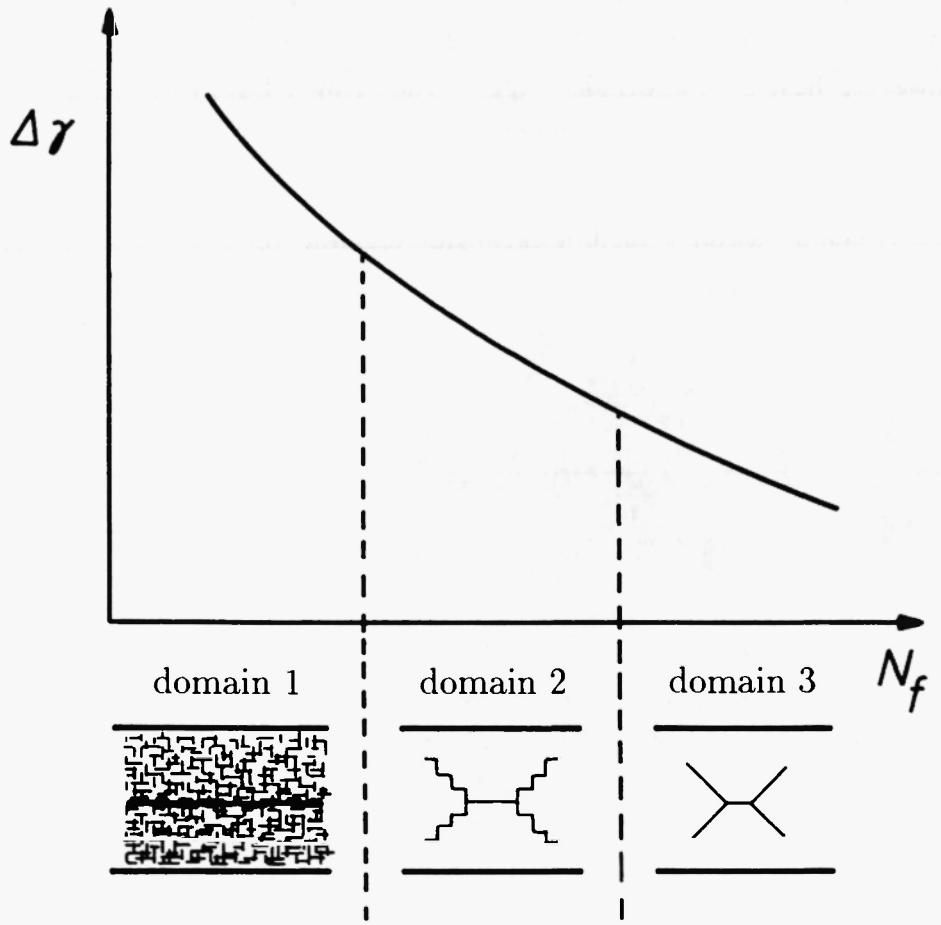

Figure 10: Schematic diagram of the shape of fatigue cracks during torsion in StE-70.

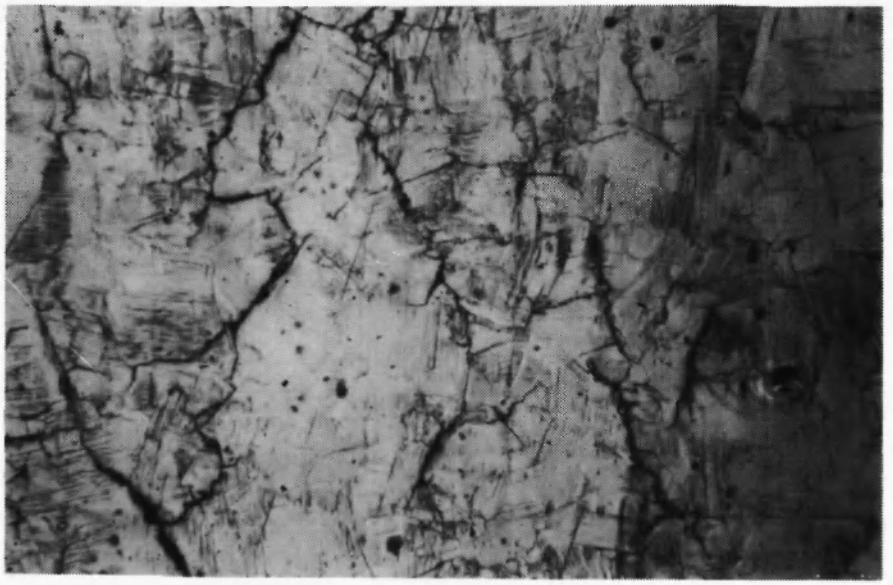

Figure 11: Crack growth in X6 CrNi 18 11 during torsion
$\Delta\gamma/2 = 1.5 * 10^{-3}$, $N_{1\ mm} = 119000$.

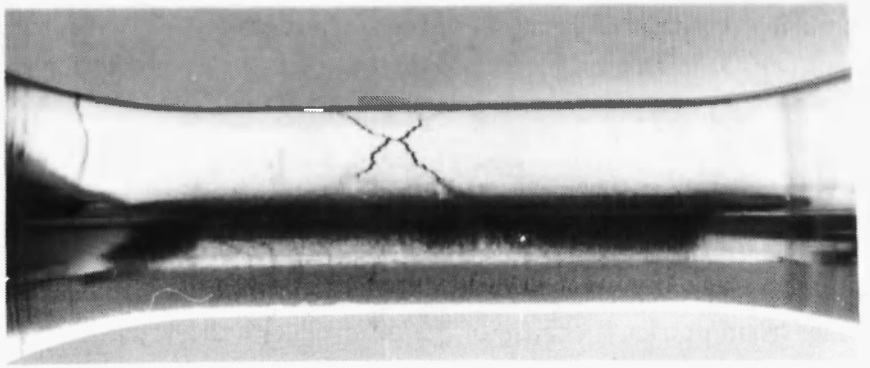

Figure 12: Crack in X6 CrNi 18 11 after torsion
$\Delta\gamma/2 = 1.5 * 10^{-3}$, $N_{1\ mm} = 119000$.

3.3.1 Biaxial Tension-Torsion Loading

When a tensile stress is superimposed onto the torsion, the plane of maximum shear is rotated and the principal stresses on both maximum normal stress planes become different. Stage I crack growth is modified accordingly. The cracks grow on

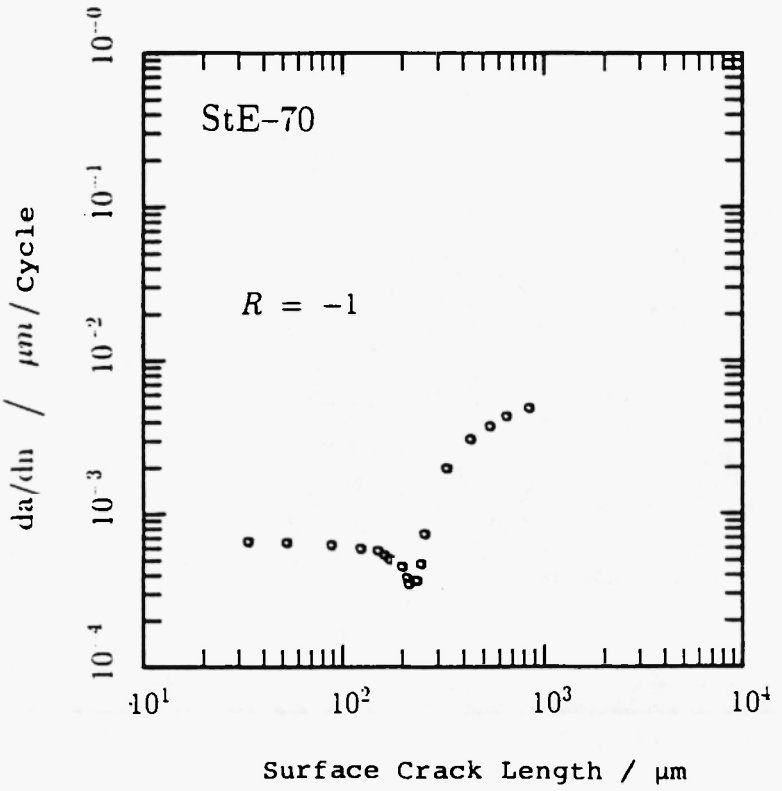

Figure 13: Crack growth rate during torsion as a function of the surface crack length $\Delta\gamma_p/2 = 3.46 * 10^{-5}$, $N_{1\ mm} = 46100$.

the inclined planes of maximum shear stress. If the amplitude is small enough to avoid crack linkage the transition to stage II growth occurs as expected: The branching configuration becomes asymmetrical because of the difference in the magnitude of the principal stresses. When the biaxiality is small enough the second branching is completely suppressed. **Figure 14** shows an example of such a crack at various stages of development. Also the crack growth rate is similar to that shown in figure 13.

At a biaxiality of $\lambda_\sigma = 0.3$ the behaviour becomes very similar to that observed in maximum tension: The trace of the crack on the surface is almost perpendicular to the tensile axes inspite of the fact that the fracture surface is inclined inwards by about 45°. The change to a maximum normal stress plane occurs in the interior of the specimen. Also the crack growth becomes similar to push-pull tests [11] in which the retardation of short cracks is less pronounced (**figure 15**).

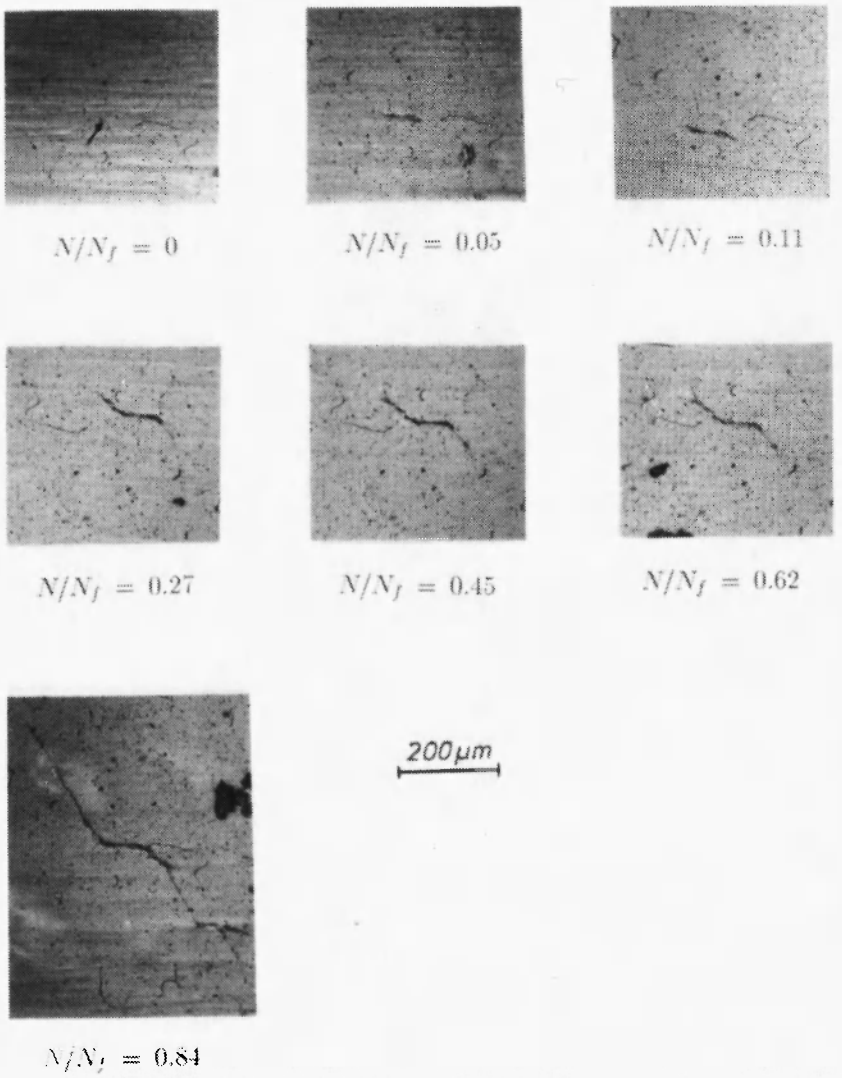

Figure 14: Fatigue crack growth in StE-70

$\Delta\bar{\epsilon}_p/2 = 8 * 10^{-5}$, $\lambda_{\epsilon_p} = 4$, $\lambda_\sigma = 1.3$, $N_{1\,mm} = 140000$

3.3.2 Treatment of crack growth with the ΔJ-Integral

For materials which show Masing behaviour the ΔJ-integral is a measure of the driving force for crack growth under cyclic loading. In a previous study [11] it was shown that crack growth in cyclic push-pull tests can be described by a power law dependence on the effective ΔJ-integral.

$$da/dN = C_J \Delta J_{eff}^{\alpha} \tag{7}$$

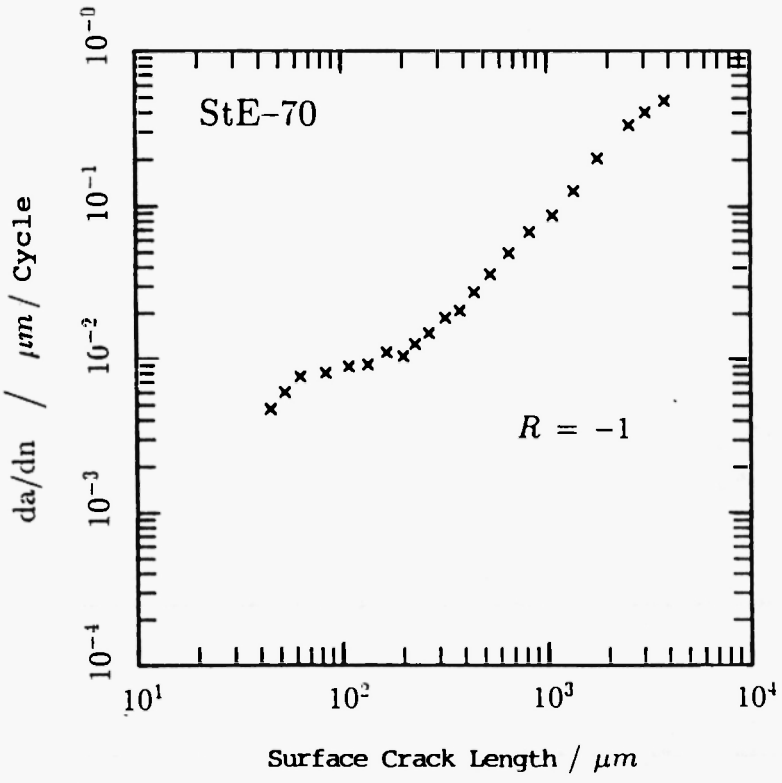

Figure 15 Crack growth rate during biaxial loading

$\Delta\bar{\epsilon}_p/2 = 2 * 10^{-4}$, $\lambda_\sigma = 0.3$, $\lambda_{\epsilon_p} = 1.73$, $N_{1\,mm} = 45800$

Rewriting the ΔJ-integral for proportional multiaxial experiments is straight forward by using the complete stress and strain tensors and results for tension-torsion in

$$\Delta J_{eff} = \left[2.9\left(\frac{\Delta\sigma_{eff}^2}{2E} + \frac{\Delta\tau_{eff}^2}{2G}\right) + 2.3\left(\frac{\Delta\sigma\,\Delta\epsilon_p}{1+n} + \frac{\Delta\tau\,\Delta\gamma_p}{1+n'}\right)\right] * a \qquad (8)$$

where n and n' are the hardening exponents of the stress-range strain-range power law for tension and torsion. For both steels used in this study we have n = n' and the values may be taken from figure 6. It is assumed that crack closure reduces the elastic ranges only [11]. In torsion the closure is independent of the sign of the shear stress. For the tensile term in (8) closure data which were obtained earlier were used. For torsion the crack closure effect was determined indirectly by performing torsion experiments with a mean torque. The reduction in life was found to be independent of the sign of the mean torque. Therefore, the inverse amplitude ratio

$$\rho_\tau = \frac{\tau_{mean}}{\Delta\tau/2} \tag{9}$$

was used to express the effective shear stress range as a function of the total shear stress range $\Delta\tau$ and the absolute value of ρ_τ. The quantitative relation which fits best to the data if given by

$$\Delta\tau_{eff} = \Delta\tau * 0.350(|\rho_\tau| + 0.055)^{0.191} \tag{10}$$

In **figure 16** the crack growth is plotted as a function of ΔJ_{eff} for the ferritic steel as determined from experiments with constant plastic strain amplitude. The tensile data are taken from [11]. The push-pull, torque and biaxial data are coincident for $\Delta J_{eff} > 250\,J/m^2$ and fall on a common line. These data refer to stage II growth which is obviously characterized by a power law dependency on ΔJ. The values of the constants of the power law are given in **figure 16.**

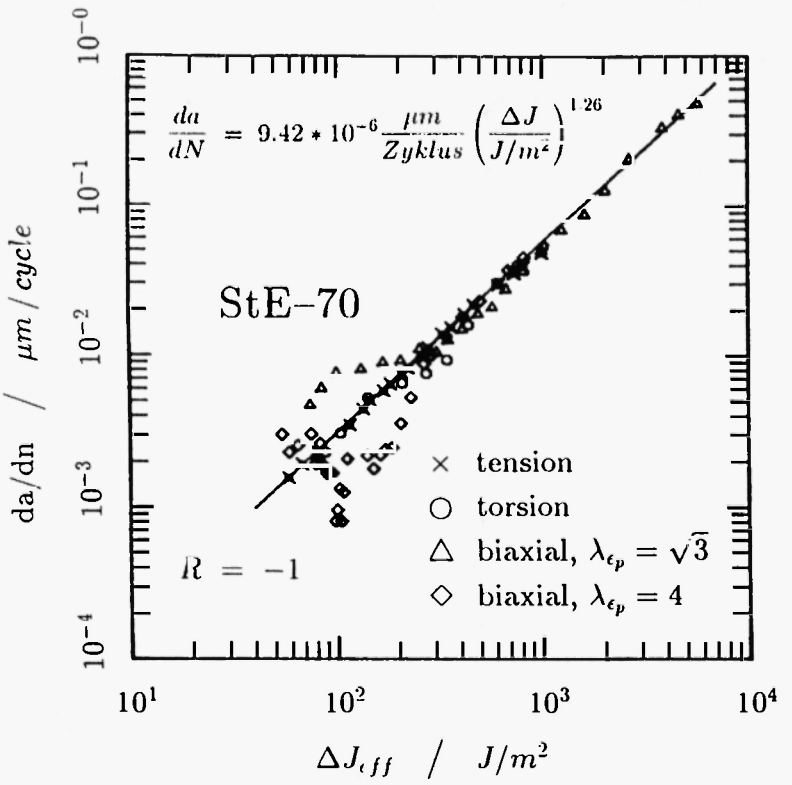

Figure 16: Crack growth rate as a function of the effective ΔJ integral for the steel StE-70 at various strain biaxialities and loading amplitudes.

The fast growth of small cracks is usually contributed to the lack of crack closure at short cracks [20]. Ebi [18] has shown that this is not sufficient to explain the fast growth in the austenite. Obviously, the fast growth is also due to the favourable conditions for crack growth at those places at which crack initiation takes place due to microstructural inhomogenities.

3.4 Life-time Predictions

In this study N_f is defined as the number of cycles necessary to produce a crack with a surface length of 1 mm. This is in contrast to [11,18] where a crack **depth** of 1 mm is used. For comparison, the life-time data were converted to the above definition of this paper. A plot of the life curves according to Coffin/Manson is shown in **figure 17**. For comparing push-pull, torsion and biaxial data the amplitude of the plastic equivalence strain was used. Obviously, there are significant differences between push-pull and torsion tests.

The ferritic steel (**figure 18**) shows a more complicated behaviour. Again there are differences between push-pull and torsion tests. Therefore it must be concluded

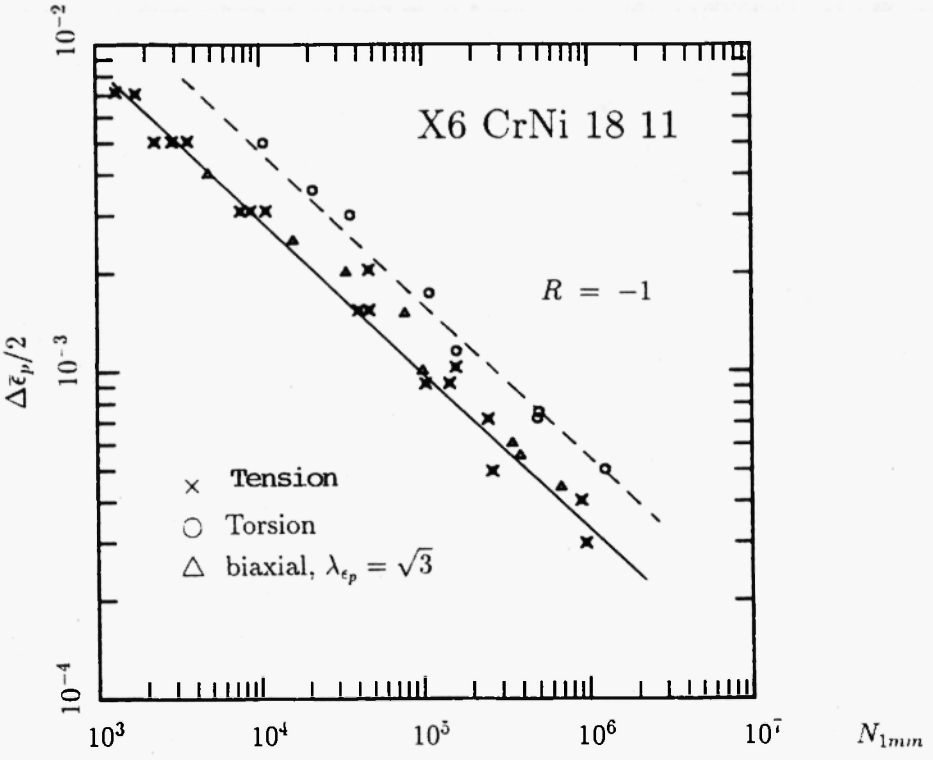

Figure 17: Coffin/Manson plot of the life data of X6 CrNi 18 11.

that for both steels the equivalent plastic strain range is not sufficient to account for the life data.

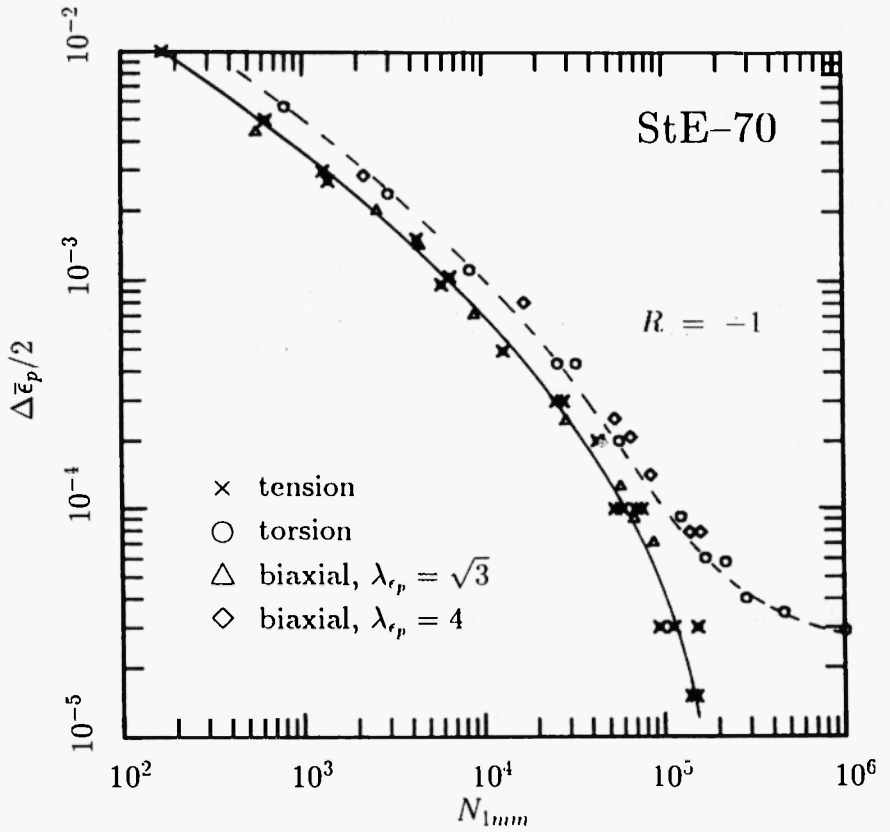

Figure 18: Coffin/Manson plot of the life data of StE-70.

3.4.1 Life-time prediction based on the ΔJ-integral.

Since crack growth can be described reasonably well by the ΔJ-integral (cf. figure 16) the life data may be plotted against the corresponding damage parameter

$$Z_D = \Delta J_{eff}/a \tag{11}$$

where ΔJ_{eff} is given by equation (8). In **figure 19** the life data from the experiments with constant plastic strain amplitude are given. Obviously, the data from push-pull, torsion and biaxial tests fall on a common line which can be described quantitatively for the ferritic steel as

$$N_{1mm} = 4.77 * 10^{12} \left(\frac{Z_D}{J/m^2}\right)^{-1.46} \tag{12}$$

The scatter in figure 18 is about 30%. For $N_{1mm} > 10^5$ cycles the elastic contributions to Z_D dominate. This explains why there are no deviations in the high-cycle fatigue range in figure 19 in contrast to the Coffin/Manson-law in figure 18. It is important to notice that no empirical adjustments had to be made to describe the life data of the various experiments with one common line. This may be due to the fact that the Z_D is a physically meaningful parameter suitable to describe the driving force on a crack under cyclic loading.

4 Conclusions

1) The cyclic stress strain curves depend only mildly on biaxiality. Cyclic deformation behaviour can be approximated by the Masing behaviour if stabilized hysteresis loops are used.

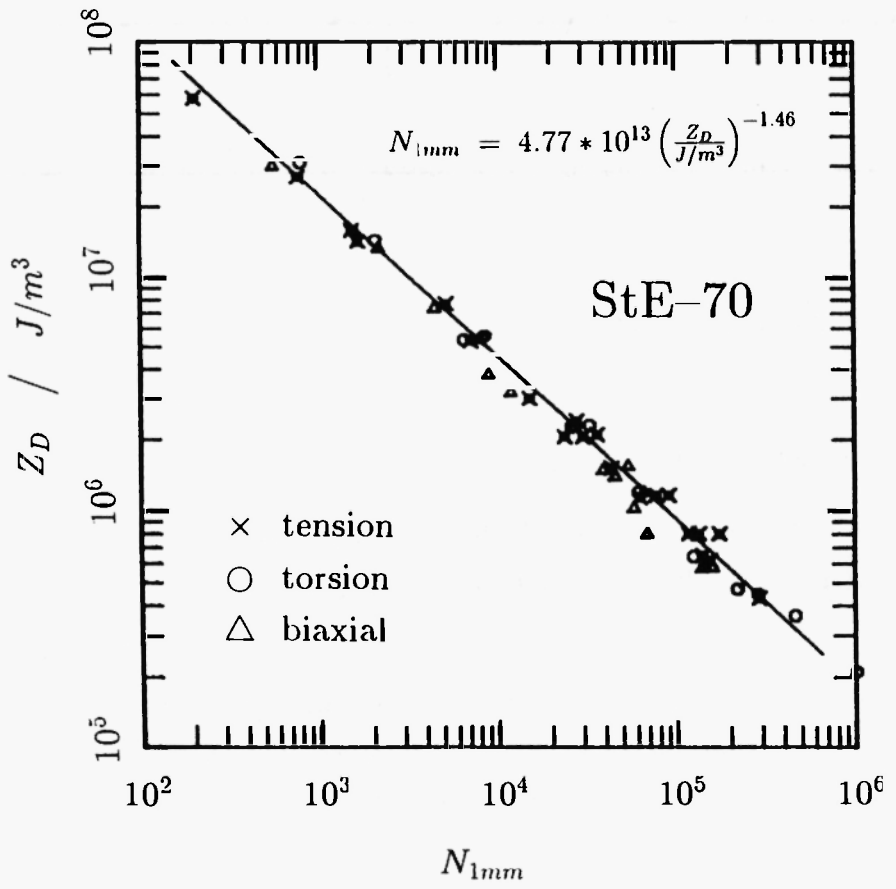

Figure 19: Relation between life time and the damage parameter Z_D for the steel StE-70.

2) Crack initiation occurs in the ferritic steel within the first 10 % of the life. Thus crack growth determines the fatigue life. In the austenitic stainless steel crack initiation at the fatigue limit occurs preferentially at twin boundaries also under biaxial loading.

3) The fast growth of small cracks on shear stress planes is nearly independent of crack length. Long cracks grow along the planes of maximum normal stress. At the transition from small to long cracks a reduced crack growth is observed.

4) The usual expression for the ΔJ integral was extended to the biaxial case with the help of equivalent stresses and strains. Beyond a critical crack length crack growth rate was found to be proportional to a power of the ΔJ integral. If the life is plotted against the damage parameter $Z_D = \Delta J_{eff}/a$, the data fall on a universal line independent of biaxiality and amplitude. Therefore, life predictions can be made for biaxial loading cases by referring exclusively to uniaxial data.

5) For random loading the life prediction is possible with an uncertainty of 50 %.

5 References

[1] Brown M.W. and Miller K.J., A Theorie for Fatigue Failure under Multiaxial Stress-Strain Conditions, Proc. Instn mech. Engrs, Vol.187, pp.745-755, 1973

[2] Lohr R.D. and Ellison E.G., Biaxial High Strain Fatigue Testing of 1Cr-Mo-V Steel, Fatigue of Engineering Materials and Structures, Vol.3, pp. 19-37, 1980

[3] Kandil F.A., Brown M.W. and Miller K.J., Biaxial Low-Cycle Fatigue Fracture or 316 stainless steel at Elevated Temperatures, The Metals Society, Vol.280, pp.203-210, London, 1982

[4] Socie D.F., Waill L.A. and Dittmer D.F., Biaxial Fatigue of Inconel 718 Including Mean Stress Effects, Multiaxial Fatigue, ASTM 853, K.J.Miller and M.W.Brown, Eds., American Society for Testing and Materials, Philadelphia, pp.463-481, 1985

[5] Krempl E., Multiaxial Fatigue - Present and Future Methods of Correlation, A.G.A.R.D. Conference Proceedings, No.155, pp. 5.1-5.12, August 1974

[6] Garud Y.S., A New Approach to the Evaluation of Fatigue under Multi-axial Loadings, in Proceedings of the Symposium on Methods for Predicting Ma-

terial Life in Fatigue, Eds. W.J.Ostergren, and J.R.Whitehead, The American Society of Mechanical Engineers, New York, pp.247-264, 1979

[7] Ellyin F., Cyclic Strain Energy Density as a Criterion for Multiaxial Fatigue Failure, Biaxial and Multiaxial Fatigue, Eds. Brown M.W. and Miller K.J., EGF 3, Eng. Publications, London, pp.571-583, 1989

[8] Dowling N. and Begley J., ASTM STP 590, American Society for Testing and Materials, pp.82-103, 1976

[9] Dowling N.E.,Crack Growth During Low-Cycle Fatigue of Smooth Axial Specimens, Cyclic Stress-Strain and Plastic Deformation Aspects of Fatigue Crack Growth, ASTM STP 637, pp.97-121, 1977

[10] Wüthrich C., The Extension of the J-Integral Concept to Fatigue, Int. Journ. Fract., Vol.20, PP.35-37, 1982

[11] Heitmann H.H., Betriebsfestigkeit von Stahl: Vorhersage der technischen Anrisslebensdauer unter Berücksichtigung des Verhaltens von Mikrorissafben, Dissertation RWTH Aachen, 1983

[12] DeLange R.G., Plastic-Replica Methods Applied to a Study of Fatigue Crack Propagation in Steel 35 CD 4 and 26 St Alluminium Alloy, Trans. TMS-AIME, Vol.230, pp.644-648, 1964

[13] Heroux L.G. and Sullivan C.P., Trans.ASM, Vol.56, pp.861-863, 1963

[14] Nadai A.,Theory of Flow and Fracture of Solids, 2nd edition, Vol.1, Ch.21 (McGraw-Hill Book Co., New York), 1950

[15] Neumann P. and Prochotta J., Shear Stresses in Thick Walled Tubular Specimens under Torsion, to be published

[16] Ebi G., Ausbreitung von Mikrorissen in duktilen Stählen, Dissertation RWTH Aachen, 1987

[17] Tönnessen A, Ermüdungsrißbildung an Cu-Polykristallen, Dissertation RWTH Aachen, 1987

[18] Neumann P. and Tönnessen A., Cyclic Deformation and Crack Initiation, Proc. Conf. Fatigue, Vol.1, pp.3-22, Charlotsville USA, 1987

[19] Bannantine J.A. and Socie D.F., Observations of Cracking Behavior in Tension and Torsion Low Cycle Fatigue, Low Cycle Fatigue, ASTM STP 942, pp.

899-921, H.D.Solomon, G.R.Haltfort, L.R.Kaisland, and B.N.Leis, Eds., American Society for Testing and Materials, Philadelphia, 1988.

[20] Schubert R., Verformungsverhalten und Rißwachstum bei Low Cycle Fatigue, Forschungsberichte VDI, Reihe 18: Mechanik/Bruchmechanik, Nr.73, 1989